

1 Multi-instrument observations of large-scale  
2 atmospheric gravity waves/traveling ionospheric  
3 disturbances associated with enhanced auroral activity  
4 over Svalbard

5 Zama T Katamzi-Joseph<sup>1,2,\*</sup>, Anasuya L Aruliah<sup>3</sup>, Kjellmar Oksavik<sup>4,5</sup>, John  
6 Bosco Habarulema<sup>1,2</sup>, Kirsti Kauristie<sup>6</sup>, Michael J Kosch<sup>1,7,8</sup>

---

7 **Abstract**

This study reports on observations of **atmospheric gravity waves/traveling ionospheric disturbances (AGWs/TIDs)** using Global Positioning System (GPS) total electron content (TEC) and Fabry-Perot Interferometer's (FPI) intensity of oxygen red line emission at 630 nm measurements over Svalbard on the night of 6 January 2014. TEC TIDs have primary periods ranging between 29 and 65 minutes and propagate at a mean horizontal velocity of  $\sim 749\text{--}761$  m/s with azimuth of  $\sim 345^\circ\text{--}347^\circ$  (which corresponds to poleward propagation direction). **On the other hand, FPI AGWs have much larger periods of  $\sim 128\text{--}174$  minutes (i.e 2.1–2.9 hours).** These large-scale AGWs/TIDs were linked to enhanced auroral activity identified from co-located all-sky camera and IMAGE magnetometers. **Similar periods, speed and poleward propagation were found for all-sky camera ( $\sim 41\text{--}49$  minutes,  $\sim 823$  m/s) and IMAGE magnetometers ( $\sim 32\text{--}53$  minutes and  $\sim 708$  m/s). Joule heating as a result of particle precipitation was identified as a likely generation mechanism for these disturbances.**

8 *Keywords:* atmospheric gravity waves, traveling ionospheric disturbances,  
9 substorm, aurora, Arctic polar cap, ANGWIN

---

\*Corresponding author

*Email addresses:* [zkatamzi@sansa.org.za](mailto:zkatamzi@sansa.org.za) (Zama T Katamzi-Joseph), [anasuya@star.ucl.ac.uk](mailto:anasuya@star.ucl.ac.uk) (Anasuya L Aruliah), [Kjellmar.Oksavik@uib.no](mailto:Kjellmar.Oksavik@uib.no) (Kjellmar Oksavik), [jhabarulema@sansa.org.za](mailto:jhabarulema@sansa.org.za) (John Bosco Habarulema), [Kirsti.Kauristie@fmi.fi](mailto:Kirsti.Kauristie@fmi.fi) (Kirsti Kauristie), [mkosch@sansa.org.za](mailto:mkosch@sansa.org.za) (Michael J Kosch)

<sup>1</sup>SANSA Space Science, Hermanus, South Africa. *Preprint submitted to Journal of LATEX Templates* July 23, 2018  
<sup>2</sup>Dept. Physics & Electronics, Rhodes University, Grahamstown, South Africa.

<sup>3</sup>Dept. Physics & Astronomy, University College London, London, UK.

<sup>4</sup>Birkeland Centre for Space Science, Dept. Physics & Technology, University of Bergen, Bergen, Norway.

<sup>5</sup>Arctic Geophysics, University Centre in Svalbard, Longyearbyen, Norway.

<sup>6</sup>Finnish Meteorological Institute, Helsinki, Finland.

<sup>7</sup>Dept. Physics, Lancaster University, Lancaster, UK.

<sup>8</sup>Dept. Physics & Astronomy, University of the Western Cape, Bellville, South Africa.

## 10 1. Introduction

11 Atmospheric gravity waves (AGWs) have been well studied for over five  
12 decades since the advent of the pioneering work by Hines (1960). Traveling  
13 ionospheric disturbances (TIDs) are signatures of AGWs in the ionosphere.  
14 AGWs/TIDs appear as wave-like perturbations in the atmospheric/thermospheric/ionospheric  
15 measurements, such as temperature, winds, plasma density and electron con-  
16 centration. These perturbations may be generated in the lower atmosphere  
17 (through processes such as mountain wave breaking, weather fronts, deep con-  
18 vection, etc) and propagate to the upper atmosphere where they eventually  
19 dissipate and may even generate secondary/tertiary waves (e.g. **Balachan-**  
20 **dran, 1980; Gall et al., 1988; Taylor and Hapgood, 1988; Fovell et al.,**  
21 **1992; Fritts and Nastrom, 1992; Satomura and Sato, 1999; Vadas**  
22 **and Liu, 2009; Becker and Vadas, 2018; Vadas et al., 2018**). Alter-  
23 natively, they may be generated in the upper atmosphere by an energy input  
24 from the magnetosphere during a magnetic substorm or storm activity (e.g.  
25 **Chan and Villard Jr., 1962; Davis, 1971; Rees et al., 1984; Hajkow-**  
26 **icz and Hunsucker, 1987; Hajkowicz, 1990; Hocke and Schlegel, 1996;**  
27 **Tsugawa et al., 2003; Ding et al., 2008; Katamzi and Habarulema,**  
28 **2014; Borries et al., 2016; Pradipta et al., 2016; Zakharenkova et al.,**  
29 **2016; Figueiredo et al., 2017; Habarulema et al., 2018**). Therefore,  
30 AGWs/TIDs are seen as a dynamical process that transport energy between  
31 different atmospheric and latitude regions, and as a result it is important to  
32 understand their properties and behaviour. In addition, since AGWs/TIDs can  
33 be accompanied by plasma instabilities that cause localised ionospheric irregu-  
34 larities (e.g. plasma bubbles), which can dramatically affect satellite-based nav-  
35 igation systems (**Hernández-Parajes et al., 2006; Nishioka et al., 2009;**  
36 **Datta-Barua et al., 2010; Yoon and Lee, 2014; Takahashi et al., 2018**),  
37 improving our understanding on AGWs/TIDs characteristics and their triggers  
38 can be useful for space weather applications.

39

40 AGWs/TIDs are commonly classified into two main groups: medium-scale  
41 and large-scale. Medium-scale AGWs/TIDs have relatively short period of 15-  
42 60 minutes, horizontal speeds and wavelengths of 100-250 m/s and less than  
43  $\sim$ 100 to 400 km, respectively, (Mayr et al., 1984). **However, more modern**  
44 **studies have extended medium-scale TIDs' horizontal wavelengths to**  
45 **1000 km (Kotake et al., 2007) and even 1500 km (Otsuka et al., 2013;**  
46 **Figueiredo et al., 2018).** The medium-scale TIDs are observed almost all  
47 the time and are mostly associated with meteorological phenomena, such as so-  
48 lar terminators, eclipses, etc. (Hernández-Parajes et al., 2006). Large-scale  
49 AGWs/TIDs have periods larger than 30 minutes, wavelengths longer than  
50 1000 km, and horizontal propagation speeds larger than 400 m/s (**Afraimovich**  
51 **et al., 2000; Ding et al., 2007; Afraimovich et al., 2013; Habarulema**  
52 **et al., 2018).** These disturbances are largely associated with disturbed mag-  
53 netic conditions, but not exclusively (Ding et al., 2008).

54  
55 Past investigations of large-scale AGWs/TIDs linked to geomagnetic dis-  
56 turbances, in particular geomagnetic storms, have largely focused on middle  
57 and low latitude events (e.g. **Hajkowicz and Hunsucker, 1987; Shiokawa**  
58 **et al., 2002; Lee et al., 2004; Hayashi et al., 2010; Ngwira et al., 2012;**  
59 **Katamzi and Habarulema, 2014; Habarulema et al., 2015; Borries**  
60 **et al., 2016; Figueiredo et al., 2017).** Even after the advent of Global Nav-  
61 igation Satellite System (GNSS), especially Global Positioning System (GPS),  
62 there has been very little work that combines optical and radio data to study  
63 the characteristics of AGWs/TIDs, particularly in the polar regions and during  
64 auroral disturbances. However, some polar AGWs/TIDs studies have been con-  
65 ducted using either optical data like airglow imagers/cameras (e.g. ) or FPI (e.g.  
66 Innis et al., 2001; Ford et al., 2006, 2008; Nicolls et al., 2012; Shiokawa et al.,  
67 2012) or satellite data (e.g. Johnson et al., 1995; Idrus et al., 2013; Momani et al.,  
68 2010) or data from radars such as ionosondes and EISCAT (European Incoherent  
69 SCATter) (e.g. MacDougall et al., 1997; Cai et al., 2011; Vlasov et al., 2011).  
70 **In particular, there are very few reported large-scale AGWs/TIDs**

71 observations from FPI measurements. For example, using a combi-  
72 nation of instruments including incoherent scatter radars and FPIs  
73 over North America and Greenland, Pi et al. (2000) reported on  
74 large-scale TIDs induced by auroral heating effects during moderate  
75 storm and substorm activities on 27-28 October 1992. Shiokawa et al.  
76 (2003) utilised measurements from a suite of instruments including  
77 an FPI at low and midlatitudes in Japan, and reported observations  
78 of equatorward large-scale TIDs caused by intense poleward winds  
79 in the lower thermosphere (90-100 km) associated with an intense  
80 storm-time substorm on 31 March 2001. Employing FPIS located  
81 in northern Scandinavia Ford et al. (2006) also observed large-scale  
82 AGWs during a tristatic campaign of 25 November 2003, although  
83 not specifically classified as a large-scale AGWs in that paper, but  
84 their reported characteristics match those of large-scale AGWs/TIDs.  
85 In a subsequent climatological study, Ford et al. (2008) reported on  
86 medium-scale and large-scale AGWs using FPIs in Sweden, Finland  
87 and Svalbard during the period of 2000-2006. They found no statisti-  
88 cal difference between solar minimum and solar maximum as well as  
89 between different geomagnetic activity levels in the number of night-  
90 time GWs observed. Using a FPI located in Poker Flat, Nicolls et al.  
91 (2012) reported on GWs activity during a period of enhanced auroral  
92 activity on 9-10 January 2010. These GWs had period, velocity and  
93 wavelength characteristics matching those in the large-scale category.

94  
95 Contrary to the high latitude case, there have been many stud-  
96 ies of AGWs/TIDs observed at lower latitudes and directly linking  
97 them to auroral sources. For examples, Davis (1971) reported that it was  
98 possible to show a connection between the occurrences of TIDs and substorms  
99 on a one-to-one basis using TEC measurements from midlatitude stations and  
100 magnetometer stations in the northern hemisphere high-latitudes. Using mea-  
101 surements from ionosondes, riometers and magnetometers, Hajkovicz and Hun-

102 sucker (1987) presented evidence that auroral particle precipitation at the start  
103 of intense geomagnetic substorms can be associated with the launching of large-  
104 scale TIDs observed at middle and low latitudes. More recently, Shiokawa et al.  
105 (2002) presented characteristics of a large-scale TID observed over midlatitude  
106 Japan from a combination of all-sky imagers, GPS and ionosondes data during a  
107 storm on 15 September 1999. They used the Sheffield University Plasmaspheric-  
108 Ionosphere Model (SUPIM), magnetic field measurements from magnetometers  
109 and UV auroral images from the Polar UVI instrument to link this disturbance  
110 to an intense auroral energy input which caused enhanced poleward neutral  
111 winds which in turn triggered the TID.

112

113 This paper reports on large-scale AGWs/TIDs observed on the night of  
114 6 January 2014 over Svalbard, which is located in the Arctic polar cap. A  
115 combination of TEC and intensity of the 630 nm red line emission measure-  
116 ments were used to determine the period and propagation characteristics of the  
117 AGWs/TIDs. In addition, we analysed auroral activity using an all-sky camera  
118 and several magnetometers to determine the origin and generation mechanisms  
119 of the observed AGWs/TIDs.

120

## 121 **2. Instrumentation and data**

122 Measurements used to study the AGWs/TIDs and to investigate their possible  
123 origin were obtained from GNSS receivers, a FPI, an all-sky camera and  
124 magnetometers in the Svalbard archipelago, namely in Spitsbergen, Hopen and  
125 Bear Island. The location of these instruments are shown in the map given in  
126 Figure 1(a). In addition, coordinates of these instruments are given in Table 1.

127

128 The TEC data in this study were calculated from GPS L1 (1575.42 MHz)  
129 and L2 (1227.60 MHz) signals at 60 s cadence. This data were collected by a  
130 set of multi-constellation NovAtel GPStation-6 receivers (NovAtel Inc., 2012)

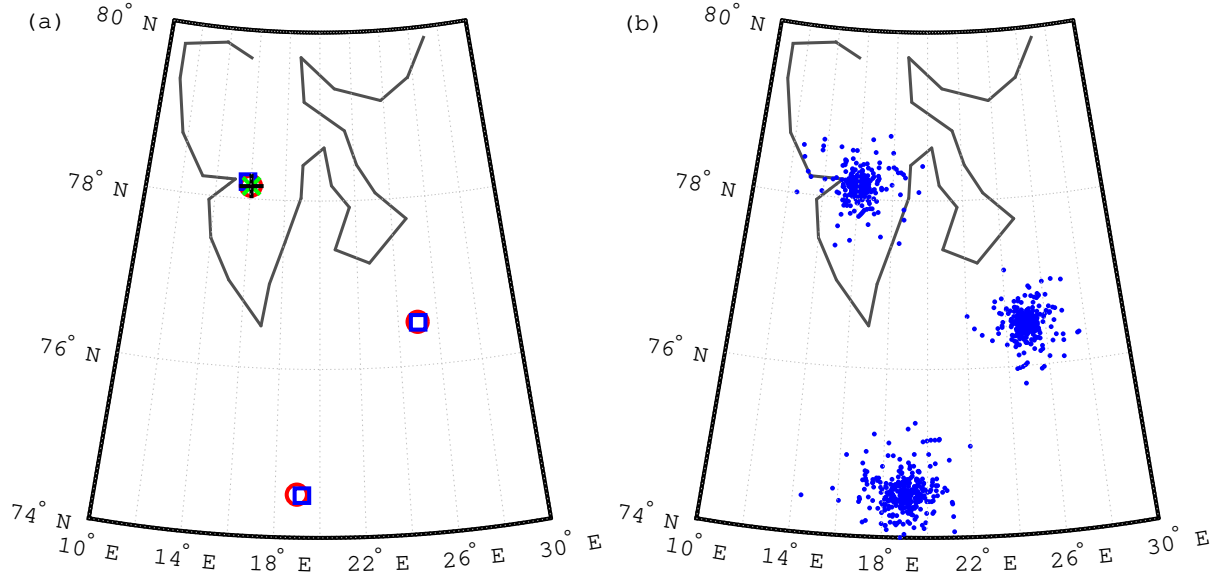


Figure 1: Maps showing: (a) locations of GNSS receivers (blue squares), FPI (green cross), all-sky camera (black plus sign) and magnetometers (red circle) used in this study;(b) ionospheric pierce points for GPS PRNs 3, 6 and 11.

131 that the University of Bergen installed in Svalbard in 2013. Data from these  
 132 receivers have been used in the past to study the poleward edge of the night-  
 133 side auroral oval (van der Meeren et al., 2015), dayside auroral forms (Oksavik  
 134 et al., 2015), and polar cap arcs (van der Meeren et al., 2016). Figure 1(b) shows  
 135 projections of ionospheric pierce points, calculated assuming the ionosphere is  
 136 a thin shell sitting at 300 km, for satellites with elevation angles greater than  
 137 30° to illustrate our TEC data spatial coverage.

138

139 Intensities of the atomic oxygen red line emission at 630 nm measured at  
 140  $\sim 9$  minutes cadence by the FPI in Longyearbyen were also used in this study.  
 141 The FPI, owned by University College London, has a field of view of 1° at  
 142 an elevation angle of 30°. More information on this instrument can be found  
 143 from Aruliah and Griffin (2001), and references therein. During the night of

Table 1: Geographic and corrected geomagnetic coordinates, in degrees, of instruments used in this study. North and East are denoted by positive latitude and longitude values, respectively.

station code	geographic latitude	geographic longitude	magnetic latitude	magnetic longitude
BJN <sup>a</sup>	74.51	19.00	71.76	106.29
HOP <sup>a</sup>	76.51	25.01	73.44	113.50
KHO/LYR <sup>b</sup>	78.15	16.04	75.52	109.93

<sup>a</sup>GNSS and magnetometer.

<sup>b</sup>GNSS, FPI, magnetometer and all-sky camera.

144 interest the FPI was observing in five look directions, namely north-east (NE),  
 145 north-west (NW), south-east (SE), south-west (SW) and zenith (ZEN). In ad-  
 146 dition, intensity keogram of 557.7 nm airglow, in 1 minute cadence, from an  
 147 all-sky camera (ASC) operating in Longyearbyen was used for this study. More  
 148 information on this type of instrument, which is part of the Magnetometer Iono-  
 149 spheric Radars All-sky Large Experiment (MIRACLE) network operated by the  
 150 Finnish Meteorological Institute (FMI), can be found in Sangalli et al. (2011).  
 151 **Lastly, measurements of the X-component of the magnetic field from**  
 152 **the International Monitor for Auroral Geomagnetic Effects (IMAGE)**  
 153 **magnetometers co-located with the GPS receivers were also used to**  
 154 **determine the influence of the auroral magnetic disturbance on ob-**  
 155 **servated AGWs/TIDs. More information on the IMAGE magnetome-**  
 156 **ter network can be found in Guo et al. (2014).**

157

### 158 3. Results

159 Figure 2 shows auroral electrojet indices, i.e. AU, AL and AE, as well  
 160 as the polar cap index on 6-7 January 2014. The auroral electrojet indices,  
 161 first introduced by Davis and Sugiura (1966), are widely used as a measure  
 162 of **high-latitude** magnetic activity, in particular **substorm-related** activity

163 (Vennerstrøm et al., 1991). The polar cap index, instituted by Troshichev and  
164 Andrezen (1985), is derived from the Thule/Qaanaaq ground-based magnetome-  
165 ter and describes the geomagnetic disturbances related to the solar wind con-  
166 ditions in the northern polar region (Stauning, 2013; Vaasiliadis et al., 1996).  
167 From Figure 2 a few minor geomagnetic disturbances were observed to have  
168 occurred throughout this night, and especially around 18 UT when TIDs (i.e.  
169 wavelike structures) were also observed as shown in Figure 3. Figure 3 presents  
170 TEC and TEC perturbations (DTEC) between 16 and 22 UT on 6 January  
171 2014 for GPS satellites with pseudorandom noise (PRN) numbers 3, 6 and 11  
172 observed at BJN, HOP and KHO. **Although wavelike structures are also**  
173 **observed in measurements from PRNs 9, 18, 19 and 28, they are**  
174 **not as clearly defined as those in PRNs 3, 6 and 11 even when the**  
175 **background TEC is removed.** TEC perturbations were determined from  
176 removing the diurnal variation, which was estimated by a fourth order polyno-  
177 mial, similar to Valladares et al. (2009); Habarulema et al. (2016).

178

179 In order to estimate the periods of these TIDs we used Lomb-Scargle least  
180 squares frequency analysis of unevenly spaced data (Lomb, 1976; Scargle, 1982),  
181 and the results are shown in Figure 4. From this figure it is observed that  
182 the dominating periods (i.e. above 75% confidence level) vary across PRNs  
183 and slightly at different observing stations. For example, from Figure 4(a) the  
184 primary periods (above 99.99% confidence level) are 29 (KHO), 32 (BJN), 37  
185 (HOP and KHO), and 58 minutes (BJN and HOP). Similarly Figure 4(b) shows  
186 that the primary modes observed from PRN 6 measurements are 29 (KHO), 43  
187 (HOP) and 46 minutes (BJN and KHO). Lastly PRN 11 detected TIDs with  
188 primary period of 39 minutes (BJN and KHO) as seen from Figure 4(c). Note  
189 that period peaks that are too wide, i.e. half maximum full width larger than 30  
190 minutes (roughly the minimum primary mode detected), are ignored to minimise  
191 ambiguity in determining the dominant periods. In addition several secondary  
192 modes (confidence level above 75% but below 99.99%) are also detected and  
193 these have periods ranging between 14 and 65 minutes. Note that all domi-

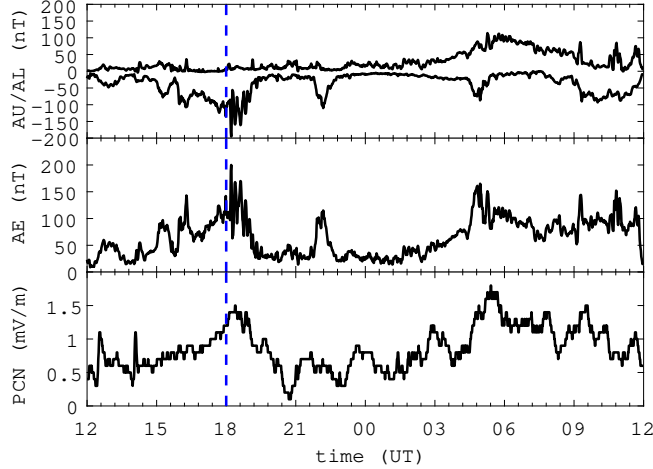


Figure 2: Auroral electrojet indices: AU and AL (top panel), AE (middle panel) and polar cap index from Thule/Qaanaaq (PCN) (bottom panel) on 6-7 January 2014. The vertical blue dash line roughly indicates occurrence of disturbances in the GPS, FPI, ASC and magnetometer measurements

194 nant periods detected from the GPS TEC are detailed in Table 2. Using the  
 195 statistical angle of arrival and Doppler method for GPS radio interferometry  
 196 (SADM-GPS), first introduced by Afraimovich et al. (1998) and also used by  
 197 Valladares and Hei (2012) and Habarulema et al. (2013), we found that these  
 198 TIDs were propagating with velocities of approximately  $760 \pm 235$ ,  $761 \pm 258$ , and  
 199  $749 \pm 267$  m/s as well as azimuths of about  $347^\circ \pm 19^\circ$ ,  $346^\circ \pm 22^\circ$ , and  $345^\circ \pm 20^\circ$   
 200 (measured clockwise from north) for waves detected by PRNs 3, 6, and 11, re-  
 201 spectively. These properties match the characteristics of large-scale TIDs (e.g.  
 202 Hocke and Schlegel (1996)).

203

204 **Figure 5(a) and (i) show intensity and wind measurements of**  
 205 **the oxygen 630 nm in several look directions taken using an FPI in**  
 206 **Longyearbyen. Although there are data gaps in some look directions**  
 207 **during the time when TIDs were identified from the GPS data, the**

Table 2: Dominant periods of TIDs detected from GPS TEC measurements.

mode	station	periods (minutes)
PRN 3		
primary	BJN	32, 58
	HOP	37, 58
	KHO	29, 37
secondary	HOP	19, 28
	KHO	65
PRN 6		
primary	BJN	46
	HOP	43
	KHO	46, 29
secondary	BJN	18, 22, 26, 33
	HOP	14, 22
PRN 11		
primary	BJN	39
	KHO	39
secondary	BJN	18
	HOP	21, 28
	KHO	25

208 intensities in the SE and SW look directions show periodic increases  
209 between 15 and 00 UT. However similar wave-like variations are not  
210 as prominent in the wind speed data, although an enhancement in  
211 the SE and SW winds is observed from around 18 UT, i.e. same  
212 time as disturbances are observed in geomagnetic indices as well as  
213 GPS data. In order to highlight intensity and wind perturbations  
214 and therefore extract AGWs/TIDs characteristics, data between 15  
215 and 21 UT was smoothed using a running 60 minute mean and the  
216 results are shown in Figure 5(b) and (ii). This figure clearly shows the  
217 presence of wave activities in both intensity and wind observations  
218 and these have larger amplitudes in the SE, SW and ZEN directions,  
219 particularly for the intensities. Lomb-Scargle analysis of the intensity  
220 and wind perturbations yields periodograms presented in Figure 5(c)  
221 and (ii), respectively. For the intensity periodogram (refer to Fig  
222 5(c)), the most dominant periods (i.e. highest power that is above  
223 75% confidence level) are approximately 107 and 56 minutes in the  
224 SW look direction, and 57 minutes in the SE look direction. The  
225 power in the wind periodogram (see Fig 5(iii)) shows a single peak  
226 at periods of 54 and 52 minutes in the SW and NE look directions  
227 respectively, while multiple peaks with a period range of 45–142 min-  
228 utes are observed for the SE and ZEN look directions (i.e. SE peaks  
229 at 59, 95 and 142 minutes and ZEN at 39 and 45 minutes). Note that  
230 there are large data gaps in the zenith, north-east and north-west  
231 look directions, and therefore period decomposition in those look di-  
232 rections is deemed not reliable. Also, periods larger than 180 minutes  
233 (3 hours) are ignored as they are greater than half the data length  
234 used to produce the periodogram and therefore are under sampled.  
235 It is noted that the majority of the dominant periods detected from  
236 this FPI data are similar those detected from GPS TEC data, but  
237 FPI also observed larger periods to those from TEC data. Propa-  
238 gation characteristics of the waves observed with FPI could not be

239 determined due to the fact that the average time delays between the  
240 SE and SW look directions (only directions with significant data for  
241 this task) are almost zero. This means that the data sampling ( $\sim 9$   
242 minutes) is too coarse/sparse and thus results in failure to resolve the  
243 wave's zonal velocity component.

244

245 Analysis of the all-sky camera keogram, presented in Figure 6(a),  
246 during the night of 6 January 2014 shows intensity brightening that  
247 stretched across the field of view at around 18 UT, which coincides  
248 with TID/AGW observations from GPS and FPI measurements. Figure  
249 6(b) shows intensities extracted at latitudes closest to the GPS  
250 stations (i.e.  $75.25^\circ$ ,  $76.58^\circ$  and  $78.15^\circ$ ) between 1730 and 1930 UT  
251 for wave period and propagation analysis. A shift in peaks at around  
252 18 UT is observed from this figure; the peak is first observed at  
253 the southern most latitude (i.e.  $75.25^\circ$ , blue curve) and last in the  
254 northern most latitude (i.e.  $78.15^\circ$ , black curve). This suggests that  
255 the auroral structure is propagating in a poleward direction. Using  
256 time delays between peaks at different latitudes and the distance be-  
257 tween observation points, we estimate a virtual horizontal velocity  
258 of  $\sim 823 \pm 143$  m/s. Figure 6(c) presents periodograms of the results  
259 presented in (b). The dominating periods were found to be  $\sim 60$  min-  
260 utes for observations at  $75.25^\circ$  as well as  $76.58^\circ$ , and  $\sim 97$  minutes for  
261 observations at  $78.15^\circ$ . It is worth noting that these properties were  
262 obtained by assuming that the 557.7 nm airglow altitude is roughly  
263 110 km. These wave periods and velocity are in agreement with  
264 those obtained for the wave-like structures observed from the GPS  
265 TEC and FPI measurements.

266

267 Figure 7(a) shows geomagnetic X-component measurements between 1730  
268 and 1930 UT, while (b) shows the same but with the baseline removed. Measure-  
269 ments for Figure 7(b) were obtained from SuperMAG ([supermag.jhuapl.edu/mag](http://supermag.jhuapl.edu/mag)),

270 where the baseline was calculated from the yearly trend in order to retain only  
271 the currents flowing in and between the ionosphere and magnetosphere (Gjer-  
272 loev, 2012). A magnetic disturbance is seen at around 18 UT in all three stations  
273 but at different times. To determine whether this disturbance may be the source  
274 of or linked to the wave-like structures seen in the GPS, FPI, and all-sky cam-  
275 era measurements, Lomb-Scargle frequency analysis and **SADM-GPS** methods  
276 were applied to the data in order to extract period and propagation information.  
277 **Note that we used SADM-GPS since the geometry of magnetometers**  
278 **is the same as the GNSS stations (i.e. magnetometers are colocated**  
279 **with GNSS receivers), but with IPP velocities set to zero since the**  
280 **measurements are stationary.** The periodograms reveal that the primary  
281 period is approximately 53 minutes for BJN and HOP observatories, and a sec-  
282 ondary period of 32 minutes for HOP. Note again that periods larger than 60  
283 minutes are ignored (for example 96 minutes for LYR station) since these peri-  
284 ods are greater than half the data length. The horizontal velocity and azimuth  
285 are estimated as  $\sim 708 \pm 261$  m/s and  $\sim 2^\circ \pm 29^\circ$  (i.e. poleward propagation), re-  
286 spectively. Again, these wave properties seems to agree with those obtained  
287 from GPS TEC and the all-sky camera.

288

#### 289 4. Discussions

290 **All the characteristics of AGWs/TIDs determined from the dif-**  
291 **ferent instruments used in this study are summarised in Table 3.**  
292 The periods and velocities are comparable to previous studies conducted at  
293 high latitudes; **for example a study by** Nicolls et al. (2012) observed grav-  
294 ity waves with a period of  $32 \pm 0.2$  minutes, horizontal phase speed of 350-770  
295 m/s and propagation direction of  $17^\circ - 50^\circ$  (**i.e. poleward direction**) dur-  
296 ing quiet conditions on 9–10 January 2010 in Alaska. Similarly, Momani et al.  
297 (2010) reported on large-scale TIDs propagating polewards at 800-1200 m/s and  
298 300-400 m/s over Antarctica during storms in October and November 2003, re-

Table 3: Summary of the wave characteristics calculated from different instruments. Note that period column shows the minimum and maximum values determined for each instrument, Vh denotes the horizontal velocity and again the minimum and maximum values (where applicable) are given, directions are given in N, NE, NW which denotes north, north-east, and north-west respectively.

Instrument	Period (min)	Vh (m/s)	Direction
GNSS/GPS	18–58	749-761	N-NW
FPI	42–142	–	–
ASC	60–97	823	N
Magnetometer	32–53	708	N

299 spectively. Also, Ford et al. (2006) observed poleward propagating  
300 large-scale AGWs with a period of 1.8 hours and horizontal velocity  
301 of 250 m/s in northern Scandinavia, which they linked to Joule heat-  
302 ing from electrojet activity. Studies by Hajkowicz and Hunsucker  
303 (1987); Yeh et al. (1994); Tsugawa et al. (2003); Lee et al. (2004);  
304 Tsugawa et al. (2004); Bruinsma and Forbes (2007); Borries et al.  
305 (2009); Pradipta et al. (2016); Figueiredo et al. (2017) have also re-  
306 ported similar results to those presented in this paper, for distur-  
307 bances linked to storm/substorm activity. The speeds are higher than  
308 some obtained from AGWs/TIDs of auroral origins observed at lower latitudes,  
309 e.g. Afraimovich et al. (2000); Habarulema et al. (2013); Ding et al. (2008), but  
310 this is expected as ion drag may reduce the speeds far from the source (Baltha-  
311 zor and Moffet, 1999).

312

313 Although a small substorm is observed around 18 UT, i.e. the AE index in  
314 Figure 2 only reaches a maximum of around 200 nT, the all-sky camera frames  
315 in Figure 8 clearly show evidence of auroral activity. This substorm/auroral  
316 activity correlates to the time of observations of AGWs/TIDs from ionospheric  
317 and thermospheric measurements. Also Figure 8 shows that the auroral arc  
318 is first seen south of the observing station (see Figure 8(a)) and quickly pro-

319 gresses north towards the station (see Figure 8(b-d)). This confirms a poleward  
320 propagation as was estimated from the keogram results in Figure 6, since both  
321 results represent the same observation but in a slightly different way. The pole-  
322 ward propagation direction is also in agreement, in general, with observations  
323 obtained from TEC and magnetic field measurements (i.e. mean azimuths of  
324 roughly  $345^\circ$  and  $2^\circ$ , respectively).

325  
326 A correlation of periods, horizontal velocities and azimuths of the wave struc-  
327 tures detected from TEC, intensity and magnetic field measurements indicates  
328 that these disturbances are related, although the measurements sample different  
329 heights of the ionosphere/thermosphere. For example, TEC measurements were  
330 calculated assuming a thin shell at  $\sim 300$  km (corresponding to typical height of  
331 the maximum electron density in the F-region), while the all-sky camera esti-  
332 mates the 557.7 nm airglow emission at  $\sim 110$  km and X-magnetic field deflec-  
333 tions infers about ionospheric currents at this same height. A study by Shiokawa  
334 et al. (2003) also reported similar velocities for their observed AGW/TIDs sam-  
335 pled at different altitudes using 630 nm airglow, TEC and virtual height mea-  
336 surements from an all-sky airglow imager, GPS, and ionosonde; they obtained  
337 velocities of 640 m/s from the all-sky imager, 370-560 m/s from GPS and 580  
338 m/s from the ionosondes. However that study was based on measurements  
339 taken in the low-middle latitudes, whereas this study used measurements from  
340 the Arctic polar cap.

341  
342 Previous investigations have indicated that the sources of large-scale TIDs  
343 in the polar regions are particle precipitation, Joule heating and Lorentz forcing  
344 (e.g. Chimona and Hines (1970); Davis (1971); hun; Hajkovicz and Hunsucker  
345 (1987)). These mechanisms result from the magnetosphere becoming inter-  
346 mittently unstable under the influence of the solar wind and depositing large  
347 amounts of energy into the polar upper atmosphere (Davis, 1971). **It is not**  
348 **possible to quantify Joule heating, particle precipitation or Lorentz**  
349 **forcing because the intensity measurements from the all-sky camera**

350 are not calibrated and there are no electric field measurements from  
351 nearby EISCAT radar for this case. However, the fact that an aurora  
352 was observed at the similar time as the AGWs/TIDs, as shown by the  
353 keogram in Figure 6 as well images presented in Figure 8, indicates  
354 that there was particle precipitation. Also, past studies have shown  
355 that the Joule heating, Lorentz forcing and particle precipitation are  
356 statistically linearly related to the AE index (Ahn et al., 1983; Wei  
357 et al., 1985), which is obtained from the horizontal magnetic field.  
358 The results presented here showed similar periods for the TEC, auroral inten-  
359 sity and the horizontal magnetic field X-component. Rice et al. (1988) studied  
360 AGW generation and propagation for a moderate geomagnetic activity event on  
361 18 October 1985 and reported that the observed AGWs had comparable peri-  
362 ods to the temporal separation of two substorms that occurred near the general  
363 source region. Also, a study on the generation, propagation and dissipation  
364 of AGWs over the European sector between 1985 and 1990 by Williams et al.  
365 (1993) found that EISCAT electric field measurements showed similar periodic  
366 modulation to the HF Doppler measurements from which gravity waves were  
367 observed. These studies showed that the TIDs and associated auroral sources  
368 may have similar periodicities, as has been observed by this study. **Therefore**  
369 **it is likely that Joule heating as a result of particle precipitation is a**  
370 **probable generation mechanism for the observed AGWs/TIDs.**

371

## 372 5. Conclusion

373 This paper presented observations of AGW/TIDs from ionospheric radio  
374 (i.e. GNSS) and thermospheric optical (i.e. FPI) measurements over Sval-  
375 bard. The periods of these disturbances varied between 14 and 174 minutes  
376 with the larger periods obtained from the FPI measurements. In addition the  
377 wave-like structures were found to propagate in a poleward direction with mean  
378 speeds of 749-761 m/s. At the same time of AGWs/TIDs observations, dis-

379 turbances in magnetometer and all-sky camera measurements in the vicinity of  
380 the AGWs/TIDs were also observed. The periods and propagation velocities of  
381 these disturbances corresponded to those of the TIDs/AGWs. **This led to the**  
382 **conclusion that the AGWs/TIDs were probably generated by Joule**  
383 **heating resulting from particle precipitation related to the observed**  
384 **auroral activity.** To the best of the authors' knowledge, this study shows the  
385 first correlation of period and propagation properties of large-scale AGWs/TIDs  
386 using radio, optical and magnetic field measurements in the Arctic polar cap.

387

### 388 **Acknowledgments**

389 For the ground magnetometer data from SuperMAG we gratefully acknowl-  
390 edge SuperMAG, PI Jesper W. Gjerloev.; The institutes who maintains the  
391 IMAGE magnetometer array, PI Liisa Juusola; The Tromsø Geophysical Obser-  
392 vatory at the University of Tromsø for operation for the three magnetometers  
393 used in this study (i.e. BJN, HOP, and LYR).

394 ZTKJ and ALA were supported by the Royal Society's Newton Advanced Fel-  
395 lowship grant NA150012. Also, KO acknowledges financial support from the  
396 Norwegian Research Council under contracts 212014 and 223252.

### 397 **References**

398 , .

399 Afraimovich, E., Astafyeva, E., Demyanov, V., Edemskiy, I., Gavriluk, N.,  
400 Ishin, A., Kosogorov, E., Leonovich, L., Lesyuta, O., Palamartchouk, K.,  
401 Perevalova, N., Polyakova, A., Smolkov, G., Voeykov, S., Yasyukevich, Y.,  
402 Zhivetiev, I., 2013. A review of GPS/GLONASS studies of the ionospheric  
403 response to natural and anthropogenic processes and phenomena. *J. Space*  
404 *Weather Space Clim.* 3, A27. doi:10.1051/swsc/2013049.

- 405 Afraimovich, E., Kosogorov, E., Leonovich, L., Palamartchouk, K., Perevalova,  
406 N., Pirog, O., 2000. Determining parameters of large-scale traveling iono-  
407 spheric disturbances of auroral origin using GPS-arrays. *J. Atmos. Sol. Terr.*  
408 *Phys.* 62, 553–565. doi:10.1016/S1364-6826(00)00011-0.
- 409 Afraimovich, E., Palamartchouk, K., Perevalova, N., 1998. GPS radio interfer-  
410 ometry of travelling ionospheric disturbances. *J. Atmos. Sol. Terr. Phys.* 60,  
411 1205–1223. doi:10.1016/S-1364-6826(98)00074-1.
- 412 Ahn, B.H., Akasofu, S.I., Kamide, Y., 1983. The joule heat production rate and  
413 the particle energy injection rate as a function of the geomagnetic indices AE  
414 and AL. *J. Geophys. Res.* 88, 6275–6287. doi:10.1029/JA088iA08p06275.
- 415 Aruliah, A., Griffin, E., 2001. Evidence of meso-scale structure in the high-  
416 latitude thermosphere. *Ann. Geophys.* 19, 37–46. doi:10.5194/angeo-19-37-  
417 2001.
- 418 Balachandran, N., 1980. Gravity waves from thunderstorms. *Mon. Weather Rev.*  
419 108, 804–816. doi:10.1175/1520-0493(1980)108<0804:GWFT>2.0.CO;2.
- 420 Balthazor, R., Moffet, R., 1999. Morphology of large-scale traveling atmo-  
421 spheric disturbances in the polar thermosphere. *J. Geophys. Res.* 104, 15–24.  
422 doi:10.1029/1998JA900039.
- 423 Becker, E., Vadas, S., 2018. Secondary gravity waves in the winter mesosphere:  
424 Results from a high-resolution global circulation model. *J. Geophys. Res.*  
425 *Atmos.* 123, 26052627. doi:10.1002/2017JD027460.
- 426 Borries, C., Jakowski, N., Wilken, V., 2009. Storm induced large scale  
427 TIDs observed in GPS derived TEC. *Ann. Geophys.* 27, 1605–1612.  
428 doi:10.5194/angeo-27-1605-2009.
- 429 Borries, C., Mahrous, A., Ellahouny, N., Badeke, R., 2016. Multiple iono-  
430 spheric perturbations during the Saint Patrick’s Day storm 2015 in the  
431 European-African sector. *J. Geophys. Res. Space Physics* 121, 11333–11345.  
432 doi:10.1002/2016JA023178.

- 433 Bruinsma, S., Forbes, J., 2007. Global observation of traveling atmospheric  
434 disturbances (TADs) in the thermosphere. *Geophys. Res. Lett.* 34, L14103.  
435 doi:10.1029/2007GL030243.
- 436 Cai, H., Yin, F., Ma, S., McCrea, I., 2011. Observations of AGW/TID prop-  
437 agation across the polar cap: a case study. *Ann. Geophys.* 29, 1355–1363.  
438 doi:10.5195/angeo-29-1355-2011.
- 439 Chan, K., Villard Jr., O., 1962. Observations of large-scale traveling iono-  
440 spheric disturbances by spaced-path high-frequency instantaneous-frequency  
441 measurements. *J. Geophys. Res.* 67, 973–988. doi:10.1029/JZ067i003p00973.
- 442 Chimona, G., Hines, C., 1970. Atmospheric gravity waves launched by auroral  
443 currents. *Planet. Space Sci.* 18, 565–582. doi:10.1016/0032-0633(70)90132-7.
- 444 Datta-Barua, S., Lee, J., Pullen, S., Luo, M., Ene, A., Zhang, G., Enge,  
445 P., 2010. Ionospheric threat parameterization for local area Global-  
446 Positioning-System-based aircraft landing systems. *J. Aircraft* 47, 1141–  
447 1151. doi:10.2514/1.46719.
- 448 Davis, M., 1971. On polar substorms as the source of large-scale  
449 traveling ionospheric disturbances. *J. Geophys. Res.* 76, 4525–4533.  
450 doi:10.1029/JA076i019p04525.
- 451 Davis, T., Sugiura, M., 1966. Auroral electrojet activity index AE  
452 and its universal time variations. *J. Geophys. Res.* 71, 785–801.  
453 doi:10.1029/JZ071i003p00785.
- 454 Ding, F., Wan, W., Ning, B., Wang, M., 2007. Large-scale travel-  
455 ing ionospheric disturbances observed by GPS total electron content dur-  
456 ing the magnetic storm of 29-30 October 2003. *J. Geophys. Res.* 112.  
457 doi:10.1029/2006JA012013.
- 458 Ding, R., Wan, W., Liu, L., Afraimovich, E., Voeykov, S., Perevalova, N., 2008.  
459 A statistical study of large-scale traveling ionospheric disturbances observed

460 by GPS TEC during major magnetic storms over the years 2003-2005. *J.*  
461 *Geophys. Res.* 113, A00A01. doi:10.1029/2008JA013037.

462 Figueiredo, C., Wrasse, C., Takahashi, H., Otsuka, Y., Shiokawa, K., Barros, D.,  
463 2017. Large-scale traveling ionospheric disturbances observed by GPS dTEC  
464 maps over North and South America on Saint Patrick's Day storm in 2015.  
465 *J. Geophys. Res. Space Physics* 122, 4755–4763. doi:10.1002/2016JA023417.

466 Figueiredo, C.A.O.B., Takahashi, H., Wrasse, C.M., Otsuka, Y., Shiokawa, K.,  
467 Barros, D., 2018. Medium-scale traveling ionospheric disturbances observed  
468 by detrended total electron content maps over Brazil. *J. Geophys. Res. Space*  
469 *Physics* 123, 22152227. doi:10.1002/2017JA025021.

470 Ford, E., Aruliah, A., Griffin, E., McWhirter, I., 2006. Thermospheric gravity  
471 waves in Fabry-Perot Interferometer measurements of the 630.0 nm OI line.  
472 *Ann. Geophys.* 24, 555–566. doi:10.5194/angeo-24-555-2006.

473 Ford, E., Aruliah, A., Griffin, E., McWhirter, I., 2008. Statistical analysis of  
474 thermospheric gravity waves from Fabry-Perot Interferometer measurements  
475 of atomic oxygen. *Ann. Geophys.* 26, 29–45. doi:10.5194/angeo-26-29-2008.

476 Fovell, R., Durran, D., Holton, J., 1992. Numerical simulations of convec-  
477 tively generated stratospheric gravity waves. *J. Atmos. Sci* 49, 1427–1442.  
478 doi:10.1175/1520-0469(1992)049<1427:NSOCGS>2.0.CO;2.

479 Fritts, D., Nastrom, G., 1992. Sources of mesoscale variability of gravity waves.  
480 Part II: Frontal, convective and jet stream excitation. *J. Atmos. Sci.* 49,  
481 111–127. doi:10.1175/1520-0469(1992)049<0111:SOMVOG>2.0CO;2.

482 Gall, R., Williams, R., Clark, T., 1988. Gravity waves generated dur-  
483 ing frontogenesis. *J. Atmos. Sci.* 45, 2204–2219. doi:10.1175/1520-  
484 0469(1988)045<2204:GWGDF>2.0CO;2.

485 Gjerloev, J., 2012. The SuperMAG data processing technique. *J. Geophys. Res*  
486 117, A09213. doi:10.1029/2012JA017683.

- 487 Guo, J., Liu, H., Feng, X., Pulkkinen, T.I., Tanskanen, E.I., Liu, C., Zhong,  
488 D., Wang, Y., 2014. Mlt and sea-sonal dependence of auroral elec-trojets:  
489 Image magnetometer network observations. *J. Geophys. Res. Space Physics*  
490 119, 3179–3188. doi:10.1002/2014JA019843.
- 491 Habarulema, J., Katamzi, Z., McKinnell, L.A., 2013. Estimating the propa-  
492 gation characteristics of large-scale traveling ionospheric disturbances using  
493 ground-based and satellite data. *J. Geophys. Res. Space Physics* 118, 7768–  
494 7782. doi:10.1002/2013JA018997.
- 495 Habarulema, J., Katamzi, Z., Yizengaw, E., 2015. First observations of  
496 poleward large-scale traveling ionospheric disturbances over the African  
497 sector during geomagnetic storms. *J. Geophys. Res. Space Physics* 120.  
498 doi:10.1002/2015JA021066.
- 499 Habarulema, J., Katamzi, Z., Yizengaw, E., Yamazaki, Y., Seemala, G., 2016.  
500 Simultaneous storm time equatorward and poleward large-scale TIDs on a  
501 global scale. *Geophys. Res. Lett.* 43, 6678–6686. doi:10.1002/2016GL069740.
- 502 Habarulema, J., Yizengaw, E., Katamzi-Joseph, Z., Moldwin, M., Buchert, B.,  
503 2018. Storm time global observations of large-scale tids from ground-based  
504 and in situ satellite measurements. *J. Geophys. Res. Space Physics* 123,  
505 711724. doi:10.1002/2017JA024510.
- 506 Hajkowicz, L., 1990. A global study of large scale traveling ionospheric distur-  
507 bances (TIDs) following a step-like onset of auroral substorms in both hemi-  
508 sphere. *Planet. Space Sci.* 38, 913–923. doi:10.1016/0032-0633(90)90058-X.
- 509 Hajkowicz, L., Hunsucker, R., 1987. A simultaneous observation of large-scale  
510 periodic TIDs in both hemispheres following an onset of auroral disturbances.  
511 *Planet. Space Sci.* 35, 785–791. doi:10.1016/0032-0633(87)90038-9.
- 512 Hayashi, H., Nishitani, N., Ogawa, T., Otsuka, Y., Tsugawa, T., Hosokava, K.,  
513 Saito, A., 2010. Large-scale traveling ionospheric disturbances observed by

514 SuperDARN Hokkaido HF radar and GPS network on 15 December 2006. *J.*  
515 *Geophys. Res.* 115, A06309. doi:10.1029/2009JA014297.

516 Hernández-Parajes, Juan, J., Sanz, J., 2006. Medium-scale traveling ionospheric  
517 disturbances affecting GPS measurements: Spatial and temporal analysis. *J.*  
518 *Geophys. Res.* 111. doi:10.1029/2005JA011474.

519 Hines, C., 1960. Internal atmospheric gravity waves at ionospheric heights. *Can.*  
520 *J. Phys.* 38, 1441–1481. doi:10.1139/p60-150.

521 Hocke, K., Schlegel, K., 1996. A review of atmospheric gravity waves and  
522 travelling ionospheric disturbances: 1982-1995. *Ann. Geophys.* 14, 917–940.  
523 doi:10.1007/s00585-996-0917-6.

524 Idrus, I., Abdullah, M., A.M., H., Husin, A., Yatim, B., 2013. Large-scale  
525 traveling ionospheric disturbances observed using GPS receivers over high-  
526 latitude and equatorial regions. *J. Atmos. Sol. Terr. Phys.* 102, 321–328.  
527 doi:10.1016/j.astp.2013.06.014.

528 Innis, J., Greet, P., Dyson, P., 2001. Evidence for thermospheric gravity waves  
529 in the southern polar cap from ground-based vertical velocity and photometric  
530 observations. *Ann. Geophys.* 19, 533–543. doi:10.5195/angeo-19-533-2001.

531 Johnson, F., Hanson, W., Hodges, R., Coley, W., Carignan, G., Spencer, N.,  
532 1995. Gravity waves near 300 km over the polar caps. *J. Geophys. Res.* 100.  
533 doi:10.1029/95JA02858.

534 Katamzi, Z., Habarulema, J., 2014. Traveling ionospheric disturbances observed  
535 at South African midlatitudes during the 29-31 October 2003 geomagnetically  
536 disturbed period. *Adv. Space. Res.* 53, 48–62. doi:10.1016/j.asr.2013.10.019.

537 Kotake, N., Y. Otsuka, T. Ogawa, T.T., Saito, A., 2007. Statistical  
538 study of medium-scale traveling ionospheric disturbances observed with the  
539 GPS networks in Southern California. *Earth Planets Space* 59, 95102.  
540 doi:10.1186/BF03352681.

- 541 Lee, C.C., Liu, J.Y., Chen, M.Q., Su, S.Y., Yeh, H.C., Nozaki, K., 2004. Ob-  
542 servation and model comparisons of the traveling atmospheric disturbances  
543 over the Western Pacific region during the 6-7 April 2000 magnetic storm. *J.*  
544 *Geophys. Res.* 109, A09309. doi:10.1029/2003JA010267.
- 545 Lomb, N., 1976. Least-squares frequency analysis of unequally spaced data.  
546 *Astrophys. and Space Sci.* 39, 447–462. doi:10.1007/BF00648343.
- 547 MacDougall, J., Hall, G., Hayashi, K., 1997. F region gravity waves in the central  
548 polar cap. *J. Geophys. Res.* 102, 14513–14530. doi:10.1029/97JA01076.
- 549 Mayr, H., Harris, I., Varisi, F., Herrero, F., 1984. Global excitation of  
550 wave phenomena in a dissipative multiconstituent medium: 1 Transfer  
551 function of the Earth’s thermosphere. *J. Geophys. Res.* 89, 10929–10959.  
552 doi:10.1029/JA089iA12p10929.
- 553 van der Meeren, C., Oksavik, K., Lorentzen, D., Paxton, L., Clausen, L.,  
554 2016. Scintillation and irregularities from the nightside part of a Sun-  
555 aligned polar cap arc. *J. Geophys. Res. Space Physics* 121, 5723–5736.  
556 doi:10.1002/2016JA022708.
- 557 van der Meeren, C., Oksavik, K., Lorentzen, D., Rietveld, M., Clausen, L., 2015.  
558 Severe and localized GNSS scintillation at the poleward edge of the nightside  
559 auroral oval during intense substorm aurora. *J. Geophys. Res. Space Physics*  
560 120, 10607–10621. doi:10.1002/2015JA021819.
- 561 Momani, M., Yatim, B., Ali, M., 2010. Large-scale traveling ionospheric distur-  
562 bances observed by GPS receivers in Antarctica. *Wuhan Univ. J. Nat. Sci.*  
563 15, 135–142. doi:10.1007/s11859-010-0210-0.
- 564 Ngwira, C., McKinnell, L.A., Cilliers, P., Yizengaw, E., 2012. An investigation  
565 of ionospheric disturbances over South Africa during the magnetic storm on  
566 15 May 2005. *Adv Space Sci.* 49, 327335. doi:10.1016/j.asr.2011.09.035.

567 Nicolls, M., Vadas, S., Meriwether, J., Conde, M., Hampton, D., 2012. The  
568 phases and amplitudes of gravity waves propagating and dissipating in the  
569 thermosphere. *J. Geophys. Res.* 117, A05323. doi:10.1029/2012JA017542.

570 Nishioka, M., Saito, A., Tsugawa, T., 2009. Super-medium-scale traveling iono-  
571 spheric disturbance observed at midlatitude during the geomagnetic storm on  
572 10 November 2004. *J. Geophys. Res.* 114, A07310. doi:10.1029/2008JA013581.

573 NovAtel Inc., 2012. GPStation-6 GNSS ionosphere scintillation and TEC  
574 monitor (GITSM) receiver user manual. Calgary, Alberta. [Available at  
575 <http://www.novatel.com/assets/Documents/Manuals/om-20000121.pdf>, Ac-  
576 cessed date 29 Mar. 2018].

577 Oksavik, K., van der Meeren, C., Lorentzen, D., Baddeley, L., Moen, J., 2015.  
578 Scintillation and loss of signal lock from poleward moving auroral forms  
579 in the cusp ionosphere. *J. Geophys. Res. Space Physics* 120, 9161–9175.  
580 doi:10.1002/2015JA021528.

581 Otsuka, Y., Suzuki, K., Nakagawa, S., Nishioka, M., Shiokawa, K., Tsugawa,  
582 T., 2013. Gps observations of medium-scale traveling ionospheric disturbances  
583 over europe. *Ann. Geophys.* 31, 163172. doi:10.5194/angeo-31-163-2013.

584 Pi, X., Mendillo, M., Hughes, W., Buonsanto, M., Sipler, D., Kelly, J., Zhou,  
585 Q., Lu, G., Hugh, T., 2000. Dynamical effects of geomagnetic storms and  
586 substorms in the middle-latitude ionosphere: An observational campaign. *J.*  
587 *Geophys. Res.* 105, 7403–7417,. doi:10.1029/1999JA900460.

588 Pradipta, R., Valladares, C.E., Carter, B.A., Doherty, P.H., 2016. Interhemi-  
589 spheric propagation and interactions of auroral traveling ionospheric distur-  
590 bances near the equator. *J. Geophys. Res. Space Physics* 121, 24622474.  
591 doi:10.1002/2015JA022043.

592 Rees, D., Smith, R., Charleton, P., McCormac, F., Lloyd, N., Steen, A., 1984.  
593 The generation of vertical thermospheric winds and gravity waves at auroral

594 latitudes - I. Observations of vertical winds. *Planet. Space Sci.* 32, 667–684.  
595 doi:10.1016/0032-0633(84)90092-8.

596 Rice, D., Hunsucker, R., Lanzerotti, L., Crowley, G., Williams, P., Craven,  
597 J., Frank, L., 1988. An observation of atmospheric gravity wave cause and  
598 effect during the October 1995 WAGS campaign. *Radio Sci.* 23, 919–930.  
599 doi:10.1029/RS023i006p00919.

600 Sangalli, L., Partamies, N., Syrjäso, M., Enell, S.F., Kauristie, K.,  
601 Mäkinen, S., 2011. Performance study of the new EMCCD-based all-  
602 sky cameras for auroral imaging. *Int. J. Remote Sens.* 32, 2987–3003.  
603 doi:10.1080/0143111.2010.541505.

604 Satomura, T., Sato, K., 1999. Secondary generation of gravity waves associ-  
605 ated with the breaking of mountain waves. *J. Atmos. Sci.* 56, 3847–3858.  
606 doi:10.1175/1520-0469(1999)056<3847:SGOGWA>2.0.CO;2.

607 Scargle, J., 1982. Studies in astronomical time series analysis: II Statistical  
608 aspects of spectral analysis of unevenly space data. *Astrophys. J.* 263, 835–  
609 853. doi:10.1086/160554.

610 Shiokawa, K., Mori, M., Otsuka, Y., Oyama, S., Nozawa, S., 2012. Mo-  
611 tion of high-latitude nighttime medium-scale traveling ionospheric distur-  
612 bances associated with auroral brightening. *J. Geophys. Res.* 117, A10316.  
613 doi:10.1029/2012JA017928.

614 Shiokawa, K., Otsuka, Y., Balan, N., Igarashi, K., Ridley, A., Knipp, D., Saito,  
615 A., Yumoto, K., 2002. A large-scale traveling ionospheric disturbance dur-  
616 ing the magnetic storm of 15 September 1999. *J. Geophys. Res.* 107, 1088.  
617 doi:10.1029/2001JA000245.

618 Shiokawa, K., Otsuka, Y., Ogawa, T., Kawamura, S., Yamamoto, M., Fukao,  
619 S., Nakamura, T., Tsuda, T., N. Balan, K.I., Lu, G., Saito, A., Yumoto, K.,  
620 2003. Thermospheric wind during a storm-time large-scale traveling iono-  
621 spheric disturbance. *J. Geophys. Res.* 108, 1423. doi:10.1029/2003JA010001.

- 622 Stauning, P., 2013. The polar cap index: A critical review of methods  
623 and a new approach. *J. Geophys. Res. Space Science* 118, 5021–5030.  
624 doi:10.1002/jgra.50462.
- 625 Takahashi, H., Wrasse, C., Figueiredo, C., Barros, D., Abdu, M., Otsuka, Y.,  
626 Shiokawa, K., 2018. Equatorial plasma bubble seeding by MSTIDs in the  
627 ionosphere. *Progress in Earth Planetary Science* 5. doi:10.1186/s40645-018-  
628 0189-2.
- 629 Taylor, M., Hapgood, M., 1988. Identification of a thunderstorm as a source  
630 of short period gravity waves in the upper atmospheric nightglow emissions.  
631 *Planet. Space Sci.* 36, 975–985. doi:10.1016/0032-0633(88)90035-9.
- 632 Troshichev, O., Andrezen, V., 1985. The relationship between interplanetary  
633 quantities and magnetic activity in the southern polar cap. *Planet. Space Sci.*  
634 33, 415–419. doi:10.1016/0032-0633(85)90086-8.
- 635 Tsugawa, T., Saito, A., Otsuka, Y., 2004. A statistical study of large-scale trav-  
636 eling ionospheric disturbances using the gps network in Japan. *J. Geophys.*  
637 *Res.* 109, A06302. doi:10.1029/2003JA010302.
- 638 Tsugawa, T., Saito, A., Otsuka, Y., Yamamoto, M., 2003. Damping  
639 of large-scale traveling ionospheric disturbances detected with GPS net-  
640 works during the geomagnetic storm. *J. Geophys. Res.* 108, 1127.  
641 doi:10.1029/2002JA009433.
- 642 Vaasiliadis, D., Angelopoulos, V., Baker, D., Klimas, A., 1996. The relation  
643 between the northern polar cap and auroral electrojet geomagnetic indices in  
644 wintertime. *Geophys. Res. Lett.* 23, 2781–2784. doi:10.1029/96GL02575.
- 645 Vadas, S., Liu, H., 2009. Generation of large-scale gravity waves and neutral  
646 winds in the thermosphere from the dissipation of convectively generated  
647 gravity waves. *J. Geophys. Res.* 114, A10310. doi:10.1029/2009JA014108.

- 648 Vadas, S., Zhao, J., Chu, X., Becker, E., 2018. The excitation of secondary  
649 gravity waves from dody forces: Theory and observation. *J. Geophys. Res.*  
650 *Atmos.* doi:10.1029/2017JD027970.
- 651 Valladares, C., Hei, M., 2012. Measurements of the characteristics of TIDs using  
652 small and regional networks of GPS receivers during the campaign of 17-30  
653 July of 2008. *Int. J. Geophys.* doi:10.1155/2012/548784.
- 654 Valladares, C., Villalobos, J., Hei, M., Sheehan, R., Basu, S., MacKenzie, E.,  
655 Doherty, P., Rios, V., 2009. Simultaneous observations of traveling ionospheric  
656 disturbances in the Northern and Southern Hemispheres. *Ann. Geophys.* 27,  
657 1501–1508. doi:10.5194/angeo-27-1501-2009.
- 658 Vennerstrøm, S., Friis-Christensen, E., Troshichev, O., Andresen, V., 1991.  
659 Comparison between the polar cap index, PC, and the auroral electrojet in-  
660 dices AE, AL, and AU. *J. Geophys. Res.* 96, 101–113. doi:10.1029/90JA01975.
- 661 Vlasov, A., Kauristie, K., Kamp, M.V.D., Luntama, J.P., 2011. A study of trav-  
662 eling ionospheric disturbances and atmospheric gravity waves using EISCAT  
663 Svalbard IPY-data. *Ann. Geophys.* 29, 2101–2116. doi:10.5194/angeo-29-  
664 2101-2011.
- 665 Wei, S., Ahn, B.H., Akasofu, S.I., 1985. The global joule heat production  
666 rate and the AE index. *Planet. Space Sci.* 33, 279–271. doi:10.1016/0032-  
667 0633(85)90059-5.
- 668 Williams, P., Virdi, T., Lewis, R., Lester, M., Rodger, A., McCrea, I., Free-  
669 man, K., 1993. Worldwide atmospheric gravity-wave study in the European  
670 sector 1985-1990. *J. Atmos. Terr. Phys.* 55, 683–696. doi:10.1016/0021-  
671 9169(93)90014-P.
- 672 Yeh, K., Ma, S., Lin, K., Conkright, R., 1994. Global ionospheric effects  
673 of the October 1989 geomagnetic storm. *J. Geophys. Res.* 99, 6201–6218.  
674 doi:10.1029/93JA02543.

- 675 Yoon, M., Lee, J., 2014. Medium-scale traveling ionospheric disturbances in  
676 the korean region on 10 November 2004: Potential impact on GPS-based  
677 navigation systems. *Space Weather* 12, 173–186. doi:10.1002/2013SW001002.
- 678 Zakharenkova, I., Astafyeva, E., Cherniak, I., 2016. GPS and GLONASS ob-  
679 servations of large-scale traveling ionospheric disturbances during the 2015  
680 St. Patrick’s Day storm. *J. Geophys. Res. Space Physics* 121, 12138–12156.  
681 doi:10.1002/2016JA023332.

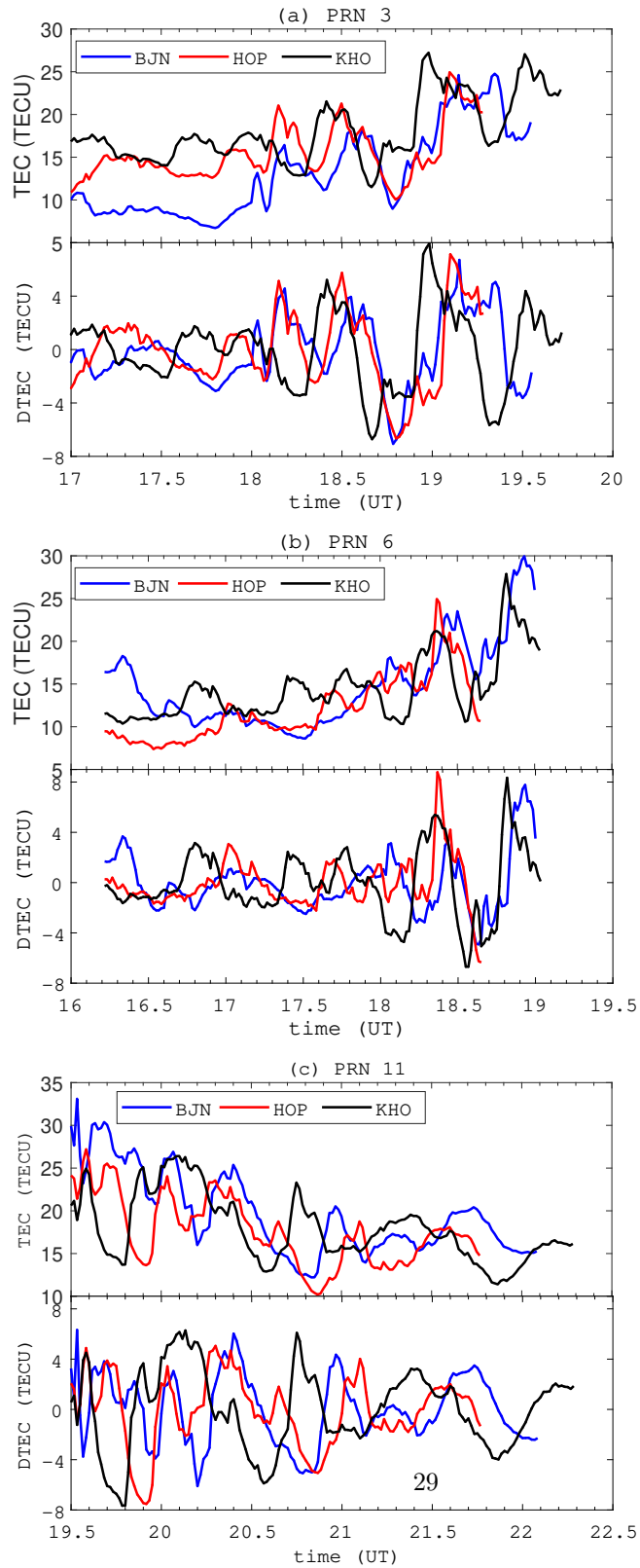


Figure 3: TEC and TEC perturbations (top and bottom panels respectively) observed with GPS PRNs (a) 3, (b) 6, and (c) 11 on 6 January 2014.

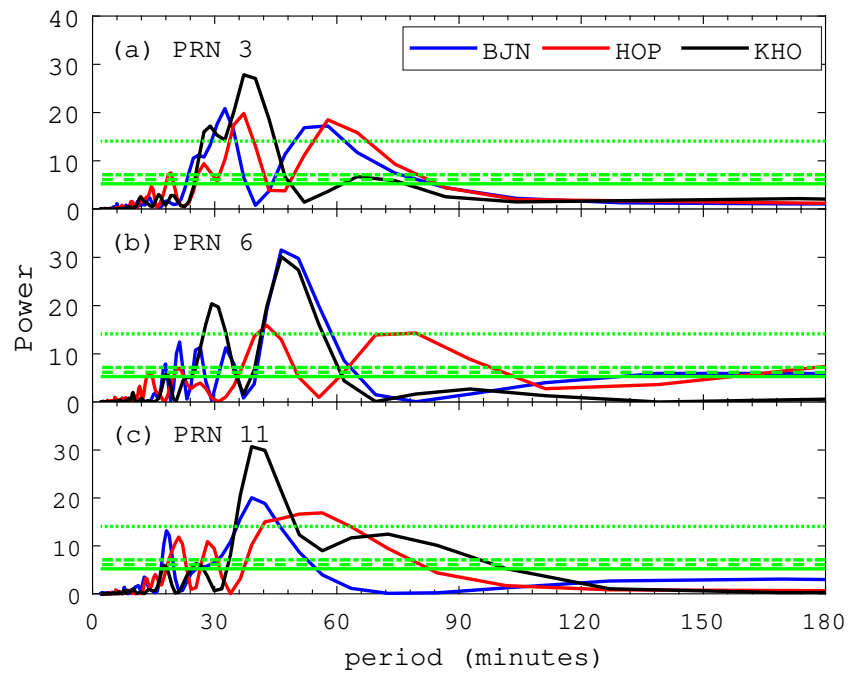


Figure 4: Periodograms of the DTEC results shown in Figure 3. The green horizontal lines show confidence levels of 99.99% (dotted line), 90% (dot-dash line), 75% (dash line), and 50% (solid line).

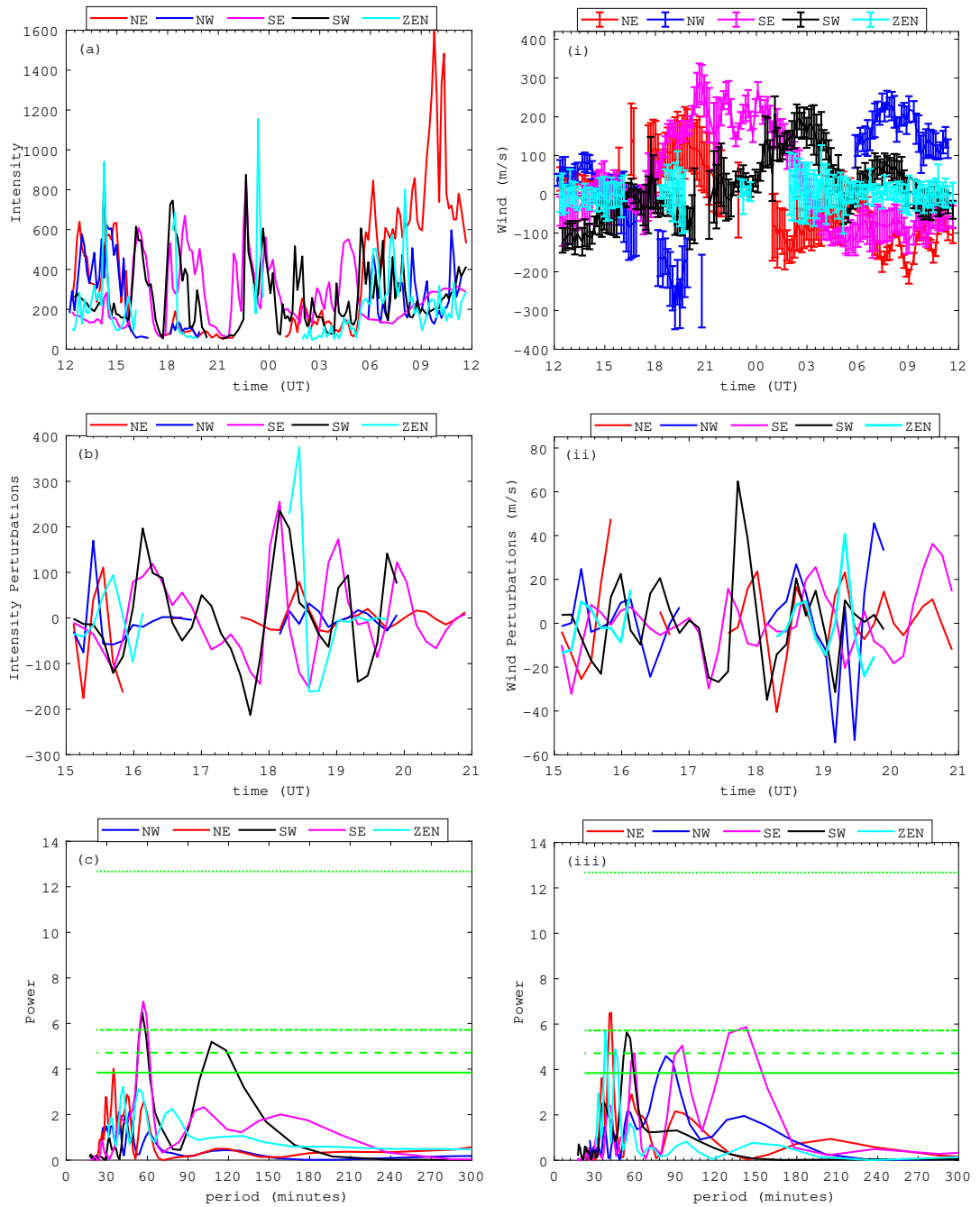


Figure 5: Variations of intensities (a) and winds(i) of 630 nm from the FPI in Longyearbyen on 6-7 January 2014. Perturbations in intensity and wind measurements (b and (ii) respectively) between 15 and 21 UT as well as their respective periodograms (c and iii). The green horizontal lines show the same confidence levels as in Figure 4.

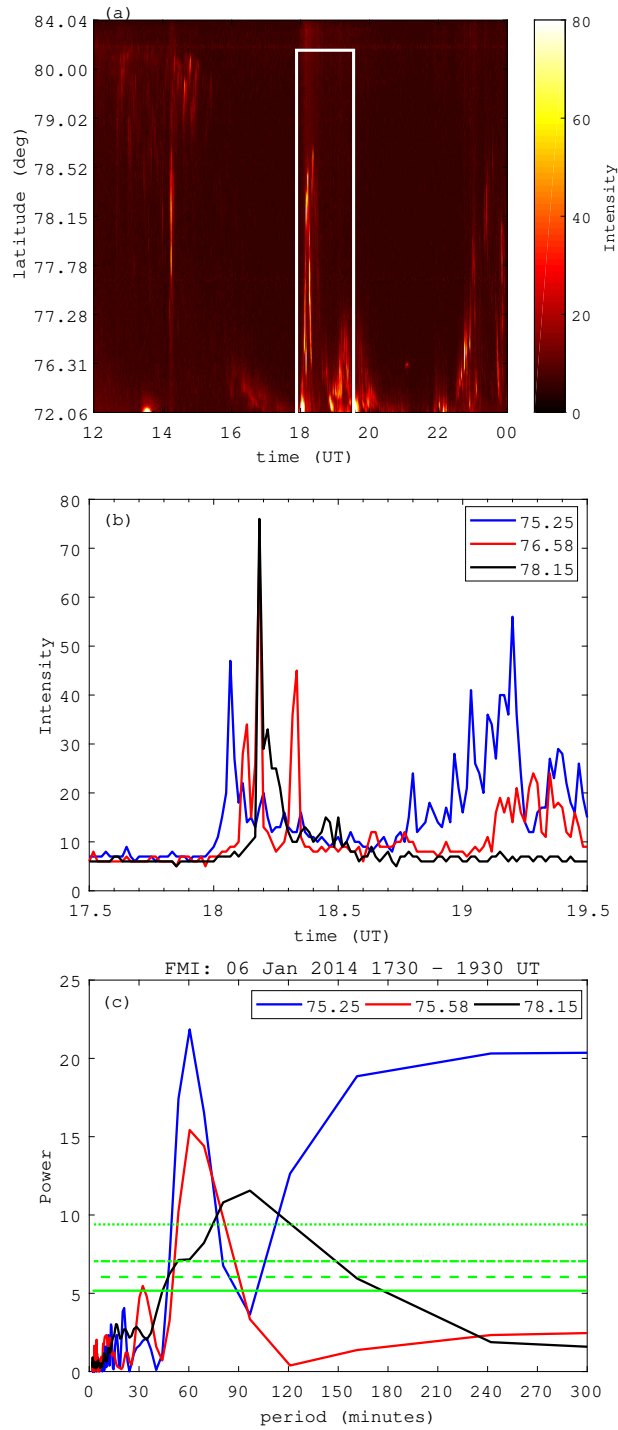


Figure 6: (a) Keogram from the all-sky camera in Longyearbyen on 6 January 2014. (b) Intensities of 557 nm wavelength between 17:30 and 19:30 UT on 6 January 2014 at different latitudes (75.25°, blue; 76.58°, red; 78.15°, black) as well as their corresponding periodograms (c). Note that the white box in (a) highlights the auroral activity of interest while green horizontal lines in (c) show the same confidence levels as in Figure 4.

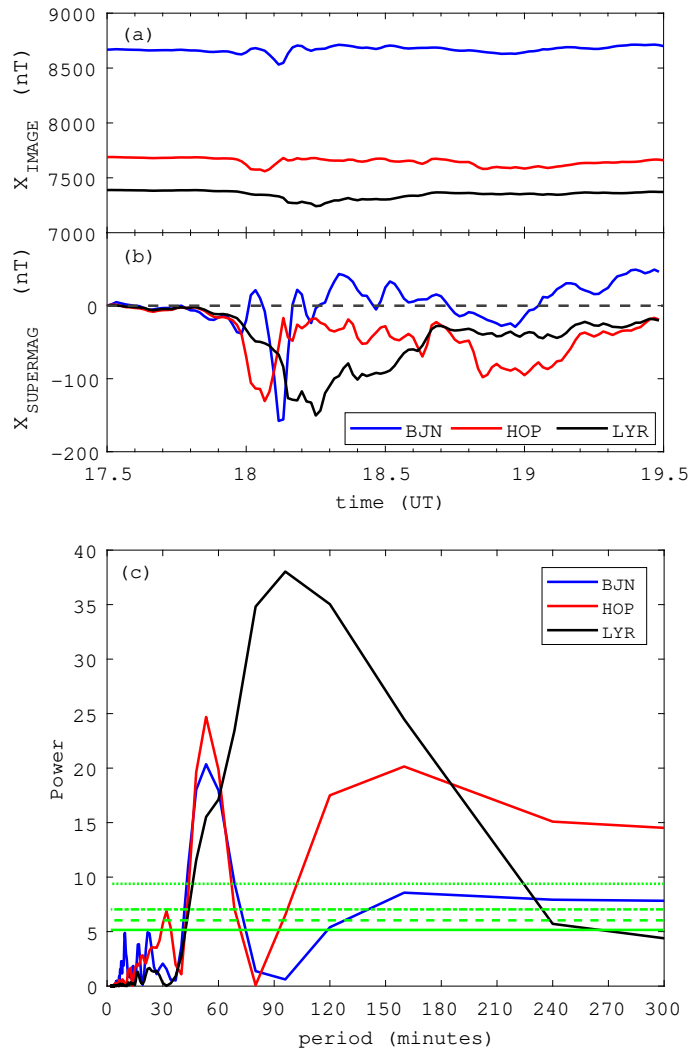


Figure 7: (a) Geomagnetic X-component, (b) X-component with baseline removed and (c) corresponding periodograms. The black dashed line in (b) show the zero  $X_{\text{SUPERMAG}}$  value and the green horizontal lines in (c) show the same confidence levels as in Figure 4.

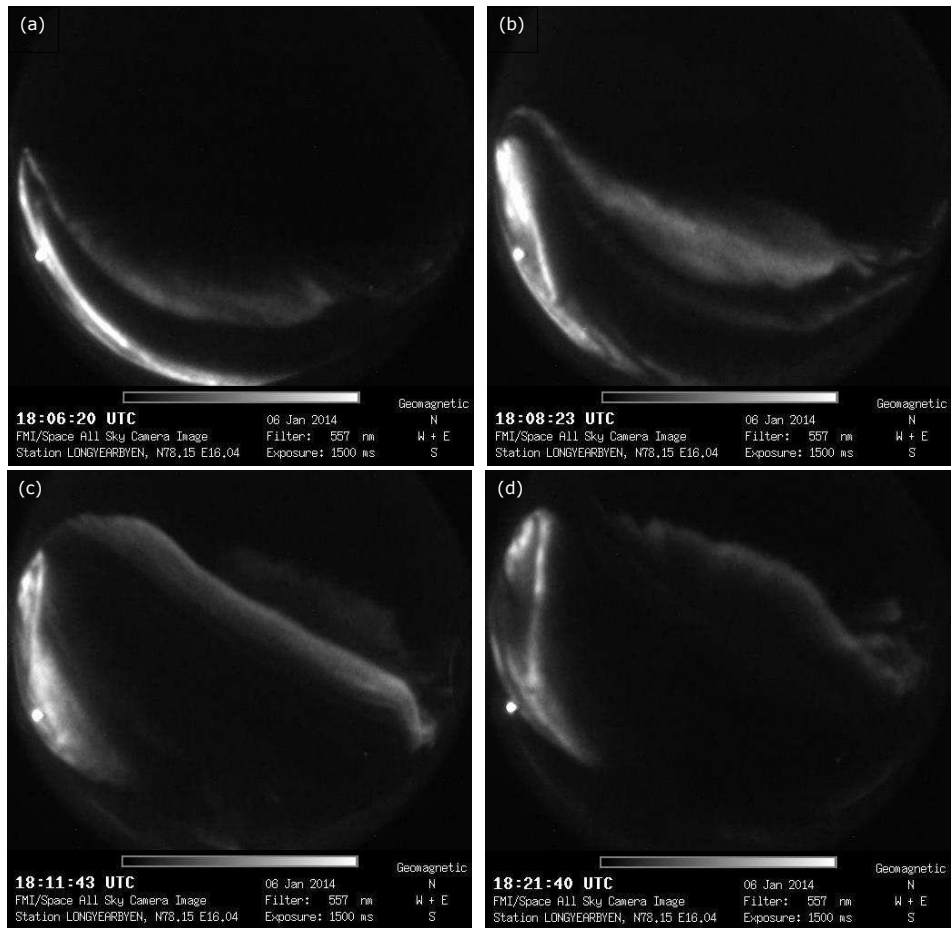


Figure 8: All-sky camera frames between 18:06 and 18:22 UT showing auroral activity at 557 nm.